ChemCatChem

Research Article
doi.org/10.1002/cctc.202500325

Chemistry Europe
European Chemical Societies Publishing

www.chemcatchem.org

Energy-Saving Dehydration of Primary Alcohol Under the Formation of Alkenes via a Bifunctional Clay Catalyst

Margherita Cavallo,[a] Adil Allahverdiyev,[b] Melodj Dosa,[a] Oscar Kelly,[c] Valentina Crocellà,[a] Francesca Bonino,*[a] and Harald Gröger*[b]

A commercial acid-leached bentonite (FULCAT®-22 F) catalyzed the dehydration of a range of alcohols efficiently under energy-saving conditions. Dehydration of a primary alcohol such as 1-hexanol took place in the 150–180 °C temperature range with a yield of 52%. This unexpected high catalytic activity was then studied by deeply characterizing the clay catalyst using both fundamental and advanced characterization methods. In agreement with VT-XRD results, by increasing the temperature, BET and PSD analysis evidenced a decrease in SSA (passing from 207 m^2 g^{-1} at 180 °C to 175 m^2 g^{-1} at 400 °C) and slight modification in the micropores present in the material (0.055 and 0.0039 cm^3 g^{-1} at 180 °C and 400 °C, respectively). EDX showed that Fe, Mg, and K are the most abundant metals present in the structure. A deep spectroscopic analysis, with different basic molecular probes (CO, CD_3CN, Py, and NH_3), revealed, by increasing the temperature, a decrease in Brønsted acid sites and an increase in Lewis acid sites. We hypothesized that the presence of these acidic sites is a key factor contributing to the observed high reaction yield of this clay-type catalyst.

1. Introduction

Without any doubts, rapid transformation of our today´s industrial raw material basis from fossil to renewable feedstocks is of utmost importance for the chemicals industry and energy sector.[1] This urgently needed change of production methods toward a renewable raw material basis will be in particular of relevance for those basic platform chemicals or commodity chemicals, which are produced on millions of tons scale. Most of those chemicals are alkenes such as ethylene and propylene, but also the higher homologous derivatives such as butenes and hexenes play an important role as bulk chemicals and offer a perspective to be used as jet fuels in the future.[2] As for the product class of hexenes, today´s typical production route is based on refining crude oil. An alternative for a future access based on CO_2 as a renewable starting material consists of Fischer–Tropsch synthesis.[3,4] However, this approach is limited by the enormous energy demand due to the needed extremely high reaction temperatures[5] but also low catalyst stability[6] and low activity as well as limited selectivity of the catalyst for such hexenes as longer carbon chain products represent drawbacks.[7] A promising further renewable-based technique represents the coupling of artificial photosynthesis with chemical dehydration. It has very recently been reported that 1-hexanol is being produced on technical scale utilizing the Siemens-Evonik process, which involves the use of CO_2 as a starting material by combining artificial photosynthesis under formation of syngas with microbial fermentation.[8] However, in spite of the realized economic access to 1-hexanol, dehydration of this primary alcohol under hexene formation remained challenging due to the high difficulty of dehydrating primary alcohols under mild conditions (in contrast to secondary and tertiary alcohols). Traditionally, very harsh conditions have been applied for dehydration of aliphatic primary alcohols, such as stoichiometric use of catalyst and reaction temperatures of > 300 °C.[9] Recently Vorholt et al. were able to show the dehydration taking place at a decreased temperature of 200 °C using phosphoric acid, however, with the ether being the main product.[10] In our very recent work aiming for decreasing the reaction temperature and increase selectivity toward alkene formation from 1-alkanols, we succeeded in obtaining yields exceeding > 70% at temperatures of 140–

[a] M. Cavallo, M. Dosa, V. Crocellà, F. Bonino
Department of Chemistry, NIS Reference Center, INSTM Research Unit, Università di Torino, Via G. Quarello 15/A and Via P. Giuria 7, Turin 10135, Italy
E-mail: francesca.bonino@unito.it

[b] A. Allahverdiyev, H. Gröger
Chair of Industrial Organic Chemistry and Biotechnology, Faculty of Chemistry, Bielefeld University, Universitätsstr. 25, Bielefeld 33615, Germany
E-mail: harald.groeger@uni-bielefeld.de

[c] O. Kelly
BYK Additives Ltd., Moorfield Road, Widnes WA8 3AA, UK

Abbreviations: BAS, Brønsted acid sites; BET, Brunauer–Emmett–Teller method; BJH, Barrett–Joyner–Halenda method; $C_7H_{13}N$, Heptanenitrile; CD_3CN, Deuterated acetonitrile; CO, Carbon monoxide; FT-IR, Fourier-transform infrared spectroscopy; LAS, Lewis acid sites; L-Py, Bands attributed to the interaction of Py with LAS; MCT, Mercury cadmium telluride cryo-detector; NH_3, Ammonia; NLDFT, Non-Local Density Functional Theory; OD, Optical density; Py, Pyridine; RT, Room temperature; SSA, Specific surface areas; STEM-EDX, Scanning transmission electron microscopy and energy dispersive X-ray analysis; TGA, Thermogravimetric analysis; VT-PXRD, Variable temperature powder X-ray diffraction; XRD, X-ray diffraction.

Margherita Cavallo and Adil Allahverdiyev contributed equally to this work.

Supporting information for this article is available on the WWW under https://doi.org/10.1002/cctc.202500325

160 °C, which represent to best of our knowledge the lowest temperatures for this reaction and, thus, energy-saving condition reported up to now. For this type of dehydration, we used either strong Lewis acids or Brønsted acids.[11] It became evident in this study, that increase of the acidity strength of the catalysts goes along with an improved catalytic performance, which is expected and can be rationalized by the increased potential to activate the hydroxy group of the primary alcohols, thus facilitating dehydration. However, these applied catalysts have been homogenous so far, which makes typically catalyst recycling and separation from product mixtures more complicated compared to the use of a heterogeneous catalyst. Thus, a heterogenous catalyst would represent a more favored option. One of the reasons why so far dehydration of primary alcohols under mild conditions is conducted with homogeneous catalysts is due to their much higher acidity, which in case of Brønsted acid catalysts often show even negative pK_a values (e.g., triflic acid). On the other hand, heterogeneous catalysts are typically less acidic. In order to overcome this limitation, we envisioned that making use of such heterogeneous catalysts, which have multiple catalytic active sites and, thus, could offer a bifunctional activation mode of the primary alcohols by an acidic activation of the hydroxy group and a basic activation of the C—H-bond in β-position, could then enable such a dehydration process in an efficient manner. The process efficiency with such a heterogeneous catalyst could then be similar or even superior to the one with homogenous catalysts and provide in addition all the advantages heterogeneous catalysis offers. In principle, various types of heterogeneous catalysts can be employed for alcohol dehydration reactions. Among the most commonly used heterogeneous catalysts are zeolites and amorphous aluminosilicates. However, these materials often exhibit notable drawbacks, including the requirement for very high reaction temperatures,[12] limited thermal stability due to decomposition through coking[13] or deactivation by water,[14] and limited selectivity as a result of promoting undesired side reactions, such as cracking or oligomerization.[15,16] In order to overcome such limitations, we became interested in studying bentonites as heterogeneous catalyst moieties in terms of their suitability due to the multiple options to fine-tune their active sites.

Bentonite is a type of claystone composed mostly of montmorillonite that is a clay mineral from the smectite group. Smectites are a group of clay minerals with a 2:1 phyllosilicate TOT structure consisting of an octahedral alumina sheet between two tetrahedral silica layers. The ideal half-cell chemical formula for montmorillonite is $M_{0.33}$, $H_2OAl_{1.67}(Fe^{2+}, Mg^{2+})_{0.33}Si_4O_{10}(OH)_2$, where M is a metal cation in the interlayer space between TOT sheets. The tetrahedral cations are Si^{4+}, and the octahedral ones are mostly Al^{3+}, Fe^{2+}, and Mg^{2+}. In the octahedral sheets, Al^{3+} is mainly replaced by Fe^{2+} and Mg^{2+}, creating an excess of negative charge in the structure. Different cations neutralize the charge and are localized in the interlayer together with water molecules.[17] This clay has been widely used, mostly in acid-leached form, in many catalytic reactions as an alternative to homogeneous catalysts, and particular attention has been paid to the study of the acidity of this material.[18–20] Typical application include the cracking process of heavy oil,[21] Friedel–Crafts acetylation,[22,23] alkylation,[24] acetylation,[25] alkyl rearrangement,[19] halogenation,[26] dimerization as well as isomerization of alkenes,[27] esterification,[28] and dehydration of alcohols toward ether[29] or alkenes.[30] As for the latter transformation, so far, bentonites have been studied for dehydration of the more reactive secondary and tertiary alcohols. In such previous studies with bentonites, however, it turned out that dehydration of secondary and tertiary alcohols toward alkenes proceeds efficiently, while for the primary alcohol, only ether formation was observable at 200 °C.[31]

From a catalytic perspective, montmorillonite exhibits both Lewis acid sites (LAS) and Brønsted acid sites (BAS), which are influenced by its provenance, the hydration level, and the thermal or acid treatment applied to the material. Usually, the LAS are associated with low-coordinated aluminium/iron/magnesium structural species or interlayer cations, while the BAS arise from structural silanols (weak acidity) and from the dissociation of interlayer water molecules coordinated the cations.[32] Since water is directly connected to the formation of BAS, the hydration level of the material plays an important role in many catalytic reactions: the higher the temperature, the lower the water content in the sample, and consequently, a lower amount of BAS is expected. On the contrary, lower temperature applications are usually associated with higher BAS content and lower LAS availability, as they are coordinated with the water molecules.[18,19]

Additionally, when an acid treatment is performed, different modifications may occur in the material, thus leading to changes in its physical properties, such as specific surface area or pore volume, and consequently in its chemical properties.[33,34] Acid-treated montmorillonite still contains a range of basic moieties, which in turn can act as a Brønsted base for proton abstraction in a dehydration process. In this case, the exchangeable cations are expected to be replaced by protons in the interlamellar space, and parallelly, the leaching of cations from octahedral sites may occur.[35,36] These treatments, therefore, probably lead to the formation of some new BAS in the structure (herein defined as "structural" BAS) different from that originated by the dissociation of the water molecules. Due to all these factors that influence the acidity of the material, it is not straightforward to make a complete identification of the different LAS and BAS.

Making use of these unique opportunities for tailoring cheap and readily available, thus economically highly attractive montmorillonite clays by adjusting acidic and basic moieties, we now developed a highly efficient process in the presence of such a catalyst for dehydration of a range of alcohols, including primary alcohols exemplified for the conversion of 1-hexanol to hexenes. It is noteworthy that in spite of having higher pKa values than the most efficient homogeneous Brønsted catalysts for theses reactions, such montmorillonite clays with bifunctional catalytic moieties outperform them in terms of catalyst loading and enables dehydration under energy-saving conditions with excellent conversion. These findings are reported in the following together with a deep characterization of the applied montmorillonite clay catalyst by means of IR spectroscopy in interaction with different probe molecules. LAS and BAS present in the

sample and their possible modification with temperature were deeply characterized allowing us to rationalize these experimentally identified outstanding catalytic activities of montmorillonite clays.

2. Materials and methods

2.1. Materials

If not otherwise stated, chemicals were procured from commercial sources and used without any further purification.

Substrates: 1-hexanol (Alfa Aesar, 99%), 2-hexanol (TCI, >98%), 2-methyl-2-hexanol (TCI, >96%), 1-heptanol (Thermo Scientific, 99%), 1-octanol (Thermo Scientific, 99%), 1-nonanol (TCI, >99%), 1-decanol (Roth, >99%).

Homogeneous catalysts: Hf(OTf)4 (Thermo Scientific, 98%), TfOH (Fluorochem, 99%), pTsOH (Thermo Scientific, >99%), AcOH (TCI, >99.5%), H_3PO_4 (85%), TFA (TCI, >99%), H_2SO_4 (Thermo Scientific, 95%–98%)

Heterogeneous catalysts: mesoporous silica (Sigma Aldrich, SBA-15), Amberchrom 50WX8 (Sigma Aldrich, H^+-form 200–400 mesh), Amberlite IR-120 (Merck, H^+-form, 15–50 mesh), Dowex (Roth, 50WX2, H^+-form, 50–100 mesh), zeolite β (abcr chemicals, ammonium-form, 680 m^2/g, 25:1 mole ratio), zeolote γ (abcr chemicals, H^+-form, 660 m^2/g, 5.2:1 mole ratio), FULCAT®-22 B and FULCAT®-22 F were provided by BYK Additives Ltd., Widnes, United Kingdom.

2.2. Catalytic Tests

Reactions were carried out under atmospheric pressure if otherwise not staed and under neat conditions, without any use of solvent. Typical reaction conditions were either in batch or distillation mode, which will be described in further detail.

Reactions were generally performed in a 25 mL flask, and a detailed experimental protocol of the dehydration experiments is given in the Supporting Information. For primary and secondary alcohols, an in situ removal by distillation was performed to shift the equilibrium to the product side. However, only for initial studies, a micro-distillation bridge was used for tertiary alcohols. Reactions were performed from 60–180 °C, depending on the substrate used. In the case of distillation, at the end of the reaction, a separation of the organic phase from the aqueous phase of the distillation flask was performed. The crude yield and alkene purities were determined by ^{1}H-NMR after determination of the mass (see Supporting Information for additional information). In case of experiments performed under batch mode, distillation was not performed. Here, at the end of the reaction, the conversion was determined using ^{1}H-NMR.

2.3. Fundamental Characterizations

Both fundamental and spectroscopic characterizations were carried out on the heterogeneous FULCAT®-22 F catalyst to better understand the reason for the high yield of the reaction. The sample was first characterized by Variable temperature powder X-ray diffraction (VT-PXRD) to study the variation in the crystalline phase by increasing the temperature. XRD patterns (CuKα) were taken using an XRD diffractometer (Malvern Panalytical, Empyrean Multicore, Detector PIXcel 3D) in the 25–400 °C temperature range (HT stage Anton Paar HTK 1200 N). During the experiment, a vacuum level of 2×10^{-2} mbar was reached, and each pattern was acquired under isothermal conditions.

Thermogravimetric analysis (TGA) was performed by means of a TA Instruments Q600 programmed using a temperature ramp of 3 °C min^{-1} from RT to 1000 °C in N_2 atmosphere (100 mL min^{-1} flows).

To check the morphology and the elemental composition of the sample, scanning transmission electron microscopy and energy dispersive X-ray analysis (FE-SEM) measurements were performed on a FESEM TESCAN S9000G equipped with a Schottky-type EGF source. The voltage used for electron acceleration is 15 kV, and the probe current is 300 pA. An OXFORD model Ultim Max Aztec software was used for the microanalysis.

N_2 adsorption/desorption isotherms were measured on a Micromeritics 3Flex at −196 °C to evaluate the textural properties of FULCAT®-22 F, previously activated at 80 °C, 180 °C, or 400 °C for 3 h under vacuum. The textural properties were evaluated by using the Microactive software provided by Micromeritics. The Specific surface area (SSA) was determined by using the Brunauer–Emmett–Teller (BET) method, over the range $P/P_0 = 0.05–0.2$, checking the Rouquerol consistency criteria.[37] The cumulative pore volume and the pore size distribution were evaluated using the Non-Local Density Functional Theory (NL-DFT), using a cylindrical pore geometry and the "NLDFT for Pillared Clays" model.

2.4. Spectroscopic Characterizations

The study of Lewis and Brønsted acidity was performed on the FULCAT®-22 F catalyst by means of Fourier-transform infrared (FT-IR) spectroscopy. The spectra were collected with a Bruker Vertex 70 equipped with an MCT (mercury cadmium telluride) cryo-detector. All the spectra were recorded in the 4500–600 cm^{-1} spectral range with a resolution of 2 cm^{-1} and an average of 32 scans. Before the analysis, FULCAT®-22 F, as a self-supported pellet, was activated in vacuum for 3 h at 80 °C, 180 °C, or 400 °C. The change in the acidic properties of FULCAT®-22 F previously evacuated at different temperatures was studied by dosing gaseous basic probe molecules on the sample. The spectral changes were detected during the adsorption/desorption of carbon monoxide (CO), deuterated acetonitrile (CD_3CN), pyridine (Py), ammonia (NH_3), and heptanenitrile ($C_7H_{13}N$). The specific experimental settings are reported elsewhere.[38–40]

3. Results and Discussion

3.1. Catalytic Tests

While dehydration of alcohols seems to be classical "textbook chemistry", such reactions are far from being established as an energy-saving, thus sustainable method for primary alcohols due

to the harsh conditions typically associated with this reaction over decades. Very recently, some of us reported the successful use of Lewis and Brønsted acids for the dehydration of such primary alcohols under relatively mild conditions, and reaction temperatures in a range of 140–160 °C.[11] Although the reusability of these catalysts for several cycles without any loss of activity was shown, various limitations remained due to the homogeneous form of these catalysts. For example, in our previous setup, quantitative removal of products was not achieved, resulting in a certain amount (10%–15%) remaining trapped inside the reaction flask. Consequently, the reaction vessel is filled after each cycle, thereby limiting the times of reuse. To overcome such limitations, we were interested in the use of heterogeneous catalysts as an alternative due to the advantages of heterogeneous catalysts in terms of simple separation and easy reuse. We chose the commercially available acid-activated clay FULCAT®-22 F as a heterogeneous catalyst, which exhibits both Lewis and Brønsted acid sites, since we envisioned that this bifunctionality enables facilitating such dehydration reactions more easily.

In order to gain insight into the potential limitations, we initially conducted a series of reactions using conventional Brønsted acids. The dehydration of 1-hexanol was selected as a model substrate due to the significance of the formed alkenes, which are, alongside ethylene and propylene, needed on large scale in the chemical industry. Reactions were performed under in-situ removal of formed hexene products at oil bath temperatures ranging between 150 and180 °C. The utilization of typical Brønsted acids with pKa values greater than 0, such as acetic acid (p*K*a 4.8), phosphoric acid (p*K*a 2.1), and trifluoroacetic acid (p*K*a 0.23), resulted in no conversion.[11] In contrast, stronger Brønsted acids, such as pTsOH or H_2SO_4,[11] also failed to yield any alkene, even at a high catalyst loading of 10 mol% (Table S1a). Instead, the much easier formation of the ether, di-*n*-hexyl ether, was observed. Since ether formation is exothermic while the alkene formation is endothermic,[41,42] these results were to be expected. For our studies we became interested in using a reduced catalyst loading of 2 mol%, which is more favorable for a large-scale application and also is in line within our previous experiments based on the utilization of metal triflates. These experiments identified several Lewis acids capable of facilitating the dehydration of primary alcohols under energy-saving temperatures.[11] It is noteworthy that even in the presence of the extremely strong Brønsted acid TfOH, which has a very low p*K*a value of −14, alkene formation was found only to a negligible extent with a very low conversion of 8% when applying a catalyst loading of 2 mol% (Scheme 1, Table S1a). Subsequently, a range of commercial heterogenous catalysts were used, stating from sulphonated Brønsted acid Dowex® where no alkene formation was observed. Using the same low catalyst loading of only 2 mol% as with TfOH, two other commercial acid catalysts, FULCAT®-22 B and FULCAT®-22 F, were tested. An high alkene yield of 23% was observed with FULCAT®-22 B but the analysis of the crude mixture revealed that, while full conversion was achieved, most of the product was di-*n*-hexyl ether (see Table S1a). By performing the same reaction using FULCAT®-22 F, which, according to BYK Additives Ltd., contains a higher proportion of BAS than FULCAT®-22 B, an improved alkene yield of 52% was achieved

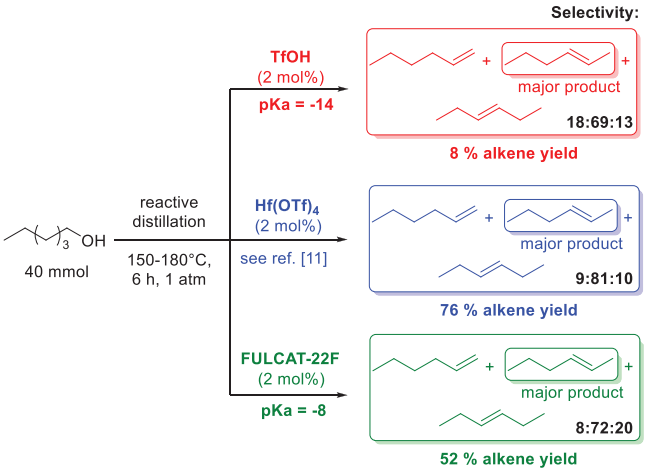

Scheme 1. Dehydration of 1-hexanol with different catalysts at a catalyst loading of 2 mol%. As Brønsted acid catalysts, TfOH and FULCAT®-22 F were utilized. The alkene yield obtained with $Hf(OTf)_4$ was reported for comparison.[11] The selectivity for the corresponding alkenes is given as a ratio (1-hexene:2-hexene:3-hexene).

(Scheme 1, Table S1a). It is noteworthy that FULCAT®-22 F has a much higher pKa value (−8) in comparison TfOH (−14), thus being much less acidic than TfOH. Acid number and pKa of the FULCAT®-series were determined by BYK Additives Ltd. and used accordingly. This surprising evidence suggests that the pKa is not the sole determining factor in the dehydration process of 1-alkanols for alkene formation. Rather these results might indicate (as a hypothesis) that the presence of both Brønsted and Lewis acid sites in FULCAT®-22 F act in synergy to reduce the activation energy required for the challenging dehydration process. It should be added that this promising alkene yield in the preliminary experiment with FULCAT®-22 F was even close to the one obtained for the dehydration when using $Hf(OTf)_4$, which turned out as the most active Lewis acid in our recent study with an alkene yield of 76% (Scheme 1).[11] However, it has to be considered that compared to the highly expensive Lewis acid $Hf(OTf)_4$, the clay FULCAT®-22 F is commercially available on large scale and, by definition, applicable in heterogeneous form. To further explore this reaction, we expanded the scope of heterogeneous catalysts. We were pleased to observe activity for some of these catalysts, as they facilitated the formation of alkenes, with Amberlite IR-120 (33%) and Amberchrom 50WX8 (34%) achieving yields comparable to FULCAT®-22 B, but still significantly lower than FULCAT®-22 F. These findings further supported our hypothesis that alkene formation depends on the synergistic interaction between BAS and LAS in heterogeneous materials.

In order too enable a comparison of these results with literature data, we have reviewed and summarized literature on the dehydration of 1-hexanol using heterogeneous catalysts (Table 1). Since, under mild conditions, the ether is the predominant product in the dehydration of primary alcohols, as we have demonstrated in our recent studies, many investigations have primarily focused on the formation of di-*n*-hexyl ether rather than alkenes. To suppress alkene formation, reactions were frequently carried out under pressurized conditions.

Table 1. Examples for the dehydration of the primary by heterogeneous catalysts in a fixed-bed reactor, a pressurized system, or under reactive distillation (1-HexOH: 1-hexanol; 1-OctOH: 1-octanol; 1-PrOH: 1-propanol).

Material	Catalyst	Method	Substrate	Temperature (°C)	Alkene Yields (%)	Reference
Alumina	η-Al_2O_3	Fixed-bed	1-HexOH	250	37 ± 3	[45]
–	γ-Al_2O_3	Fixed-bed	1-HexOH	300	42	[12]
–	γ-Al_2O_3	Fixed-bed	1-OctOH	380	45.1	[53]
–	CeO_2-doped Al_2O_3	Fixed-bed	1-HexOH	300	95	[46]
Ion-exchange resin	Amberlyst-70	Pressurized	1-HexOH	180	3.8[a)]	[43]
–	Amberlyst-15	Pressurized	1-HexOH	150	2.8[a)]	[44]
–	NR50	Pressurized	1-HexOH	180	1.0[a)]	[43]
Zeolite	H-BEA-25	Pressurized	1-HexOH	180	1.5[a)]	[43]
–	M-ZSM-5	Fixed-bed	1-PrOH	230	>97	[49]
Montmorrolinite	FULCAT®-22 F	Reactive distillation (batch)	1-HexOH	150–180 °C	52	**This work**

[a)] These numbers were calculated based on the conversion and alkene selectivity (conversion x selectivity).

For example, in the studies by Fite et al.[43] and Tejero et al.,[44] the combination of mild temperatures (150–180 °C) and pressurized systems resulted predominantly in ether formation, with alkene yields remaining below 4% in total. To obtain comparable yields to the montmorillonite sample presented in this study, the reaction temperature needed to be increased by at least 39%.[45] As the reaction temperature is above the boiling point of the alcohol, gas-phase reaction with a fixed-bed reactor was performed. Alumina is one of the most commonly used heterogeneous catalysts for dehydration reactions. Numerous studies have demonstrated its effectiveness in the dehydration of 1-hexanol, typically operating at temperatures ranging from 250 to 380 °C.[12,45–47] In contrast, ion-exchange resins are more commonly applied in ether synthesis.[43,44] Zeolites, on the other hand, have attracted considerable interest in the dehydration of lower alcohols, such as ethanol,[48] 1-propanol,[49] and 1-butanol,[50] due to their tunable acidity and shape-selective properties. [51,52]

While these findings are significant for the dehydration of primary alcohols, they do not match the potential demonstrated by montmorillonites. In our study, we achieved remarkably high yields of 52% at significantly milder reaction conditions with reaction temperatures between 150 and 180 °C.

Building on the optimization of reaction conditions in our recent work,[11] which enabled the dehydration of primary alcohols at the lowest reported temperatures of 140–160 °C, we became interested in further exploring this challenging reaction using heterogeneous catalysts.

As the dehydration of a primary alcohol has been successfully conducted by means of the clay FULCAT®-22 F at a low catalyst loading of 2 mol%, secondary and tertiary alcohols have been investigated, yielding 88% and 91%, respectively (Scheme 2, Table S2a). Both of these yields, which are obtained at a lower reaction temperature of 150 °C and 110 °C, respectively, are in a similar range to the one obtained when using the Lewis acid $Hf(OTf)_4$ as the most efficient catalyst so far.[11] However, in the case of the tertiary alcohol, the reaction time needed to be doubled to reach 91%.

Following the successful dehydration of each of these alcohols, an investigation was conducted to determine the lowest reaction temperature at which the tertiary alcohol could be dehydrated. As dehydration of this alcohol could be conducted successfully at the lowest temperature and an in situ-removal of the product was not needed, 2-methyl-2-hexanol was chosen as a model substrate (Figure 1). Consequently, the reactions were performed at temperatures between 60 and 110 °C (Figure 1B, Table S2b). While the reaction was successfully conducted at 60 °C, a quantitative conversion was not achieved. Nevertheless, increasing the temperature to 80 °C resulted in an almost quantitative conversion after three hours. It is likely that a full conversion cannot be reached under lower temperature conditions due to the occurrence of a back reaction, which leads to the formation of alcohol. Given that the tertiary carbocation is the most stable one, the tertiary alcohol will then be formed in such a back reaction (Figure 1A). We suggest that the interaction of BAS and LAS with the substrate is responsible for both the dehydration and hydration reactions. The postulated catalytic mechanism will later be further discussed in detail (Figure 5 and related text section) when describing the dehydration of a primary alcohol. In summary, FULCAT®-22 F shows the ability to dehydrate 2-methyl-2-hexanol already at 60 °C.

In a subsequent step, we also became interested in evaluating the impact of the chain length of primary alcohols on the dehydration process. It was previously reported that the alkene yield decreases with increased chain lengths when homogenous Lewis acids were used.[11] As the boiling point of the formed alkene products increased, dehydration reactions were performed under reduced pressure and such reactions were successfully conducted for C_6–C_{10}. When utilizing again 2 mol% of the clay catalyst FULCAT®-22 F, we were pleased to find constantly satisfactory alkene yields for the C_6-C_8 alkenes while a decrease was observed with $> C_8$ (Scheme 3, Table S1a).

Advantages of a heterogeneous catalyst are the easy removal from the reaction media as well also the reuse and recycling of the catalyst. Thus, we employed FULCAT®-22 F for 10 cycles. After the end of each cycle, fresh substrate was added to start the

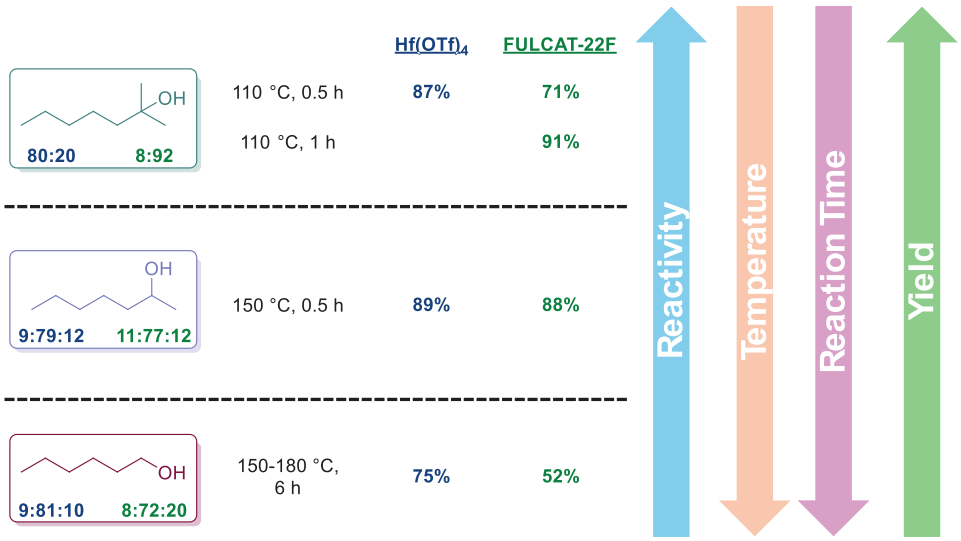

Scheme 2. Dehydration of primary, secondary, and tertiary alcohols using FULCAT®-22 F and $Hf(OTf)_4$ as reference catalyst. For the primary and secondary alcohol, the selectivity toward 1-, 2-, and 3-alkene is shown (by means of the ratio 1:2:3). For the tertiary alcohol, the selectivity toward the Saytzeff and Hofmann product is shown (S:H).

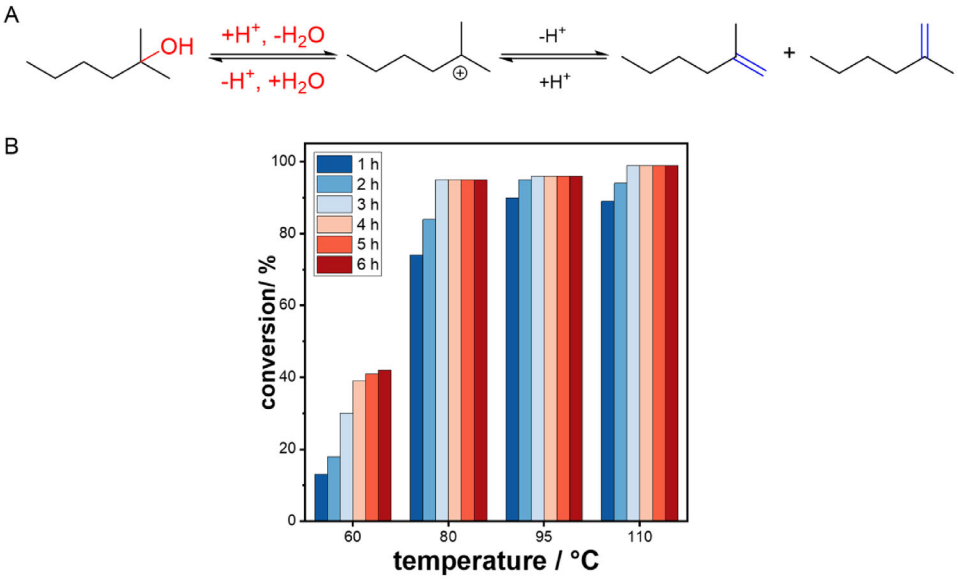

Figure 1. (A) Reaction mechanism of the dehydration and back reaction of 2-methyl-2-hexanol; (B) conversion of the dehydration of 2-methyl-2-hexanol at different reaction temperatures.

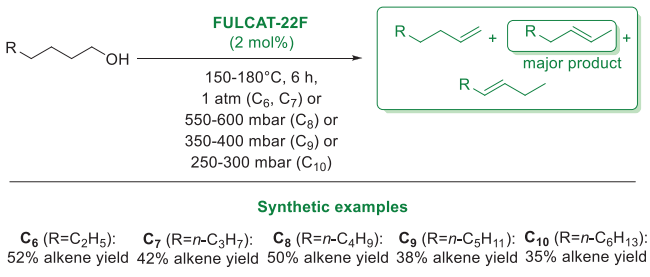

Scheme 3. Dehydration of primary alcohols with varying chain lengths by FULCAT®-22 F.

next cycle. FULCAT®-22 F was successfully used for 10 cycles without any loss of activity (Figure 2, Table S1b). An average alkene yield of 41% was obtained. The alkene yields varied throughout the cycles due to the heterogeneous nature of FULCAT®-22 F. It is hypothesized that the formed alkenes were trapped inside the pores during one cycle and then released in the next cycle. During cycle 6 to cycle 7, a recycling of the catalyst was necessary. The reaction media was then removed, and FULCAT®-22 F was repeatedly washed with solvent. While a reduced yield was determined in cycle 7, cycle 8–10 yields increased to the average number. This experiment demonstrated the reusability and recycling of FULCAT®-22 F without any loss of activity.

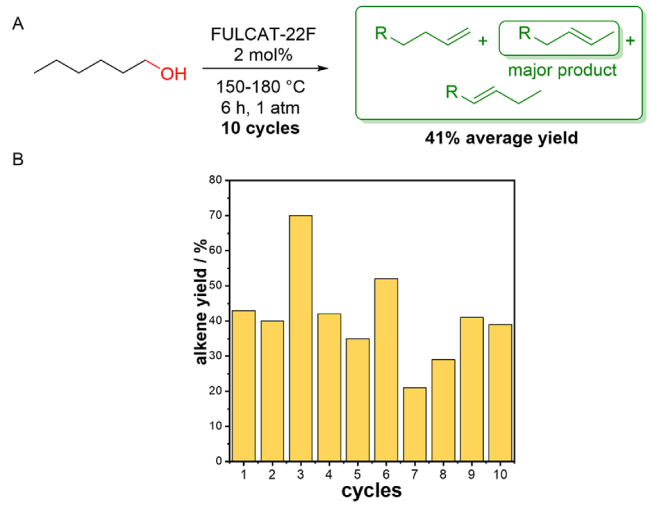

Figure 2. (A) Dehydration of primary alcohols by FULCAT®-22 F and (B) Reusability and recycling study of FULCAT®-22 F in the dehydration of 1-hexanol.

In conclusion of the synthetic experiments using FULCAT®-22 F, we could demonstrate a broad versatility of this clay-type catalyst for the dehydration of numerous alcohols. Of particular relevance and highly remarkable is the outstanding performance of this bifunctional clay catalyst containing Lewis and Brønsted acid as well as Brønsted base sites for dehydration of primary alcohols at energy-saving conditions with reaction temperatures in the range of 150–180 °C. Note that despite having a much less Brønsted acidity, FULCAT®-22 F outperforms even highly acidic catalysts such as TfOH. Thus, it was shown that a higher acidity of the catalyst is not solely responsible for an improved alkene formation, and accordingly, we also became interested in getting a deeper insight into the catalytic structure of FULCAT®-22 F. Thus, a detailed characterization of this heterogeneous FULCAT®-22 F catalyst was carried out to understand the origin of its higher performance, and the results of this catalyst characterization study are presented in the subsequent chapter.

3.2. Fundamental Characterizations

Since, as mentioned above, the H_2O content can influence both the original structural and acidic properties of the bentonite, a schematic representation of which is given in Figure 3A, the synthesized sample and its behavior upon activation at increasing temperature were first studied by means of VT-XRD (Figure 3B).

The diffractogram of the as-synthesized material at 25 °C (black curve) evidenced the presence of the main reflections associated with the montmorillonite (M) phase, together with some impurities of Quartz (Q).[54] In particular, the main characteristic reflection of montmorillonite at about 7°, corresponding to the (0 0 1) reflection, is evident at all the activation temperatures (PDF Nr. 00-003-0016). However, as the temperature increases, the main reflection peak at 7° decreases and becomes broader (from black to green curves), giving rise at higher temperatures to an additional peak at about 9°, which seems to persist even when the sample is cooled in vacuum to RT (dark gray curves). This behavior, which was already observed in the literature,[55,56] is caused by a change in the crystallographic parameters of the material during evacuation in the 25–500 °C temperature range. By comparing the diffractogram of the as-synthesized sample collected at 25 °C and the one activated at 400 °C (Figure S8), the differences in the (001) reflection become particularly evident, suggesting a decrease in the basal spacing with the temperature caused by the dehydration of the sample. Further information on the behavior of the material upon heating can be obtained by TGA analysis (Figure S9), where three different weight losses were observed, the first occurring between RT and 200 °C, is due to water removal in the structure, and perfectly agrees with VT-XRD findings (for details and further information, see Supporting Information)

The specific surface area (SSA) and pore size distribution (PSD) of the sample activated at 80 °C, 180 °C, and 400 °C were also studied (see Section 5 in the Supporting Information). These temperatures, which will also be used for the advanced characterisation (see below), were chosen to see the effect of water removal on the textural properties of the material. All three N_2 adsorption/desorption isotherms display a combination of type Ib and type IVa isotherms with a type H3 hysteresis loop (Figure S10).[57] As a matter of fact, clays exhibit three different types of porosity: (i) micropores due to the interlamellar pores localized in the interlayer span of the clay, (ii) mesopores due to intra-aggregate pores situated in between adjacent laminae piles, and (iii) macropores due to inter-aggregate pores occupying space in-between aggregates of clay particles and non-clay particles (see Figure S10 for a schematic representation).[58]

The SSA of the material showed a slight decrease passing from 180 °C to 400 °C (175 and 207 $m^2\ g^{-1}$, respectively), while an intermediate value was observed in the case of activation at 80 °C (200 $m^2\ g^{-1}$) (see Table 2 and Figures S12–S14 for the BET fit). NL-DFT model highlights the presence of both micropores and mesopores (see Figure S11, Table 2, and Figures S15–S17 for the NL-DFT fit). In particular, the NL-DFT pores size distribution (PSD) of micropores (Figure S11a) evidenced for all the three activation temperatures the presence of an homogeneous family with a size of 1.5 nm while in the case of the samples activated at 80 °C and 180 °C, an additional smaller family centered at 1 nm can also be identified. A slight decrease in the micropore volume is also observed as the activation temperature is increased to 400 °C (see Figure S11b, Table 2). Concerning the mesoporous cavities, the PSD is characterized in the 2–10 nm range by the presence of a heterogeneous family of sites (Figure S11a and Table 2). In this case, the mesopore volume showed a slight decrease passing from 180 °C to 400 °C (0.163 and 0.161 $cm^3\ g^{-1}$, respectively) while a slightly lower volume is observed in the case of the samples activated at the lowest temperature (0.158 $cm^3\ g^{-1}$) (Figure S11b and Table 2). The SSA and PSD values suggest that the interlamellar pores constantly decrease with increasing temperature, as shown by the reduction in SSA, micropores, and mesopores volumes from 180 °C to 400 °C, in perfect agreement with VT-XRD and TGA analysis. However, for the sample activated at 80 °C, the presence of residual water is probably hindering the full accessibility of the surface, leading

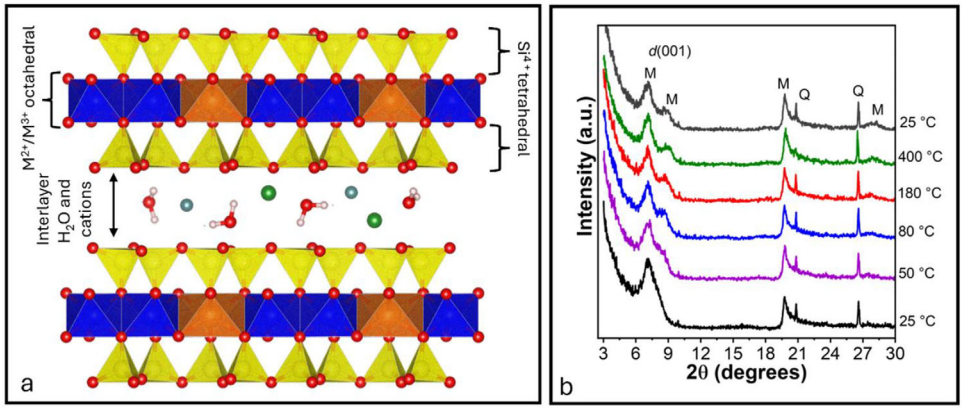

Figure 3. Pictorial representation of the original structure of bentonite (structural OH are not shown) (a) and VT-XRD of FULCAT®-22 F heating the sample in vacuum in the temperature range from 25 to 400 °C (from black to green curves) and after cooling down to 25 °C in vacuum (grey curve) (b).

Table 2. Specific surface area as determined by the BET equation and porosity (determined by the NL-DFT method) for FULCAT®-22 F activated at 400 °C, 180 °C, and 80 °C. The mesopore volume was obtained by subtracting the micropore volume from the total pore volume.

	BET area (m^2 g^{-1})	*V* total (cm^3 g^{-1})	*V* micro (cm^3 g^{-1})	*V* meso (cm^3 g^{-1})	Micropores size (nm)	Mesopores size (nm)
ACT 400 °C	175.1 ± 0.1	0.200	0.039	0.161	1.5	2–10
ACT 180 °C	207.1 ± 0.3	0.218	0.055	0.163	1 / 1.5	2–10
ACT 80 °C	200.8 ± 0.5	0.211	0.053	0.158	1 / 1.5	2–10

Table 3. Elemental composition of FULCAT®-22 Fobtained by EDX analysis.

Elements	O	Fe	Mg	K	Cu	Ca	Ti	Si/Al
Wt. %	54.78	3.83	0.94	0.40	0.30	0.38	0.36	3.27
Dev. std	0.74	0.61	0.86	0.17	0.19	0.04	0.05	2.08

to an underestimation of both the SSA and mesopore volume of the material.

In order to investigate the main elements present in the sample, FESEM-EDX analysis was performed (Figure S18 and Table 3).

The samples exhibited leaf-like crystals, which are organized in dense aggregates [55] and all the elements result in being well dispersed (Figure S18). The sample has a large variety of elements, with the prevalence of Si and Al followed by Fe, Mg, and K. Furthermore, Cu, Ca, and Ti were also observed to a lesser extent. It is worth noting that the content of elements is probably influenced by the acid treatment used to obtain the commercial sample, where a series of processes take place depending on the type and intensity of the treatment. The acid treatment is probably also responsible for the higher Si/Al ratio shown by FULCAT®-22 F with respect to the one expected from the untreated montmorillonite structure (~2).

3.3. Advanced Characterization

To investigate the presence of acidic sites in the sample, a detailed in situ IR characterization was performed. First, a preliminary analysis of the as-synthesized and evacuated sample was carried out, showing a progressive decrease in stretching and bending vibrational bands of H_2O upon increasing temperature (see Supporting Information, e.g., Figure S19, for further information).

In IR spectroscopy, it is a common procedure to completely evacuate the sample prior to the adsorption of different probe molecules.[59] However, since, as previously pointed out, the different content of water in montmorillonite can influence both the structural and acidic properties of the material, the activation temperature should be carefully selected. In this regard, three different temperatures were chosen for the activation: 80 °C, 180 °C, and 400 °C. At the first two temperatures, some interlayer water is still present in the structure. These conditions are quite close to those of one of the catalytic tests. On the other hand, the highest temperature, although not achievable during catalyst testing, represents the best activation temperature for spectroscopy since it causes the complete removal of the molecular water.

Different probe molecules with different basicity were dosed on the sample, previously activated at 80 °C and 180 °C, to study the presence and the variations of Lewis acid sites (LAS) and Brønsted acid sites (BAS), and try to correlate them with the catalytic activity of the sample. The sam-

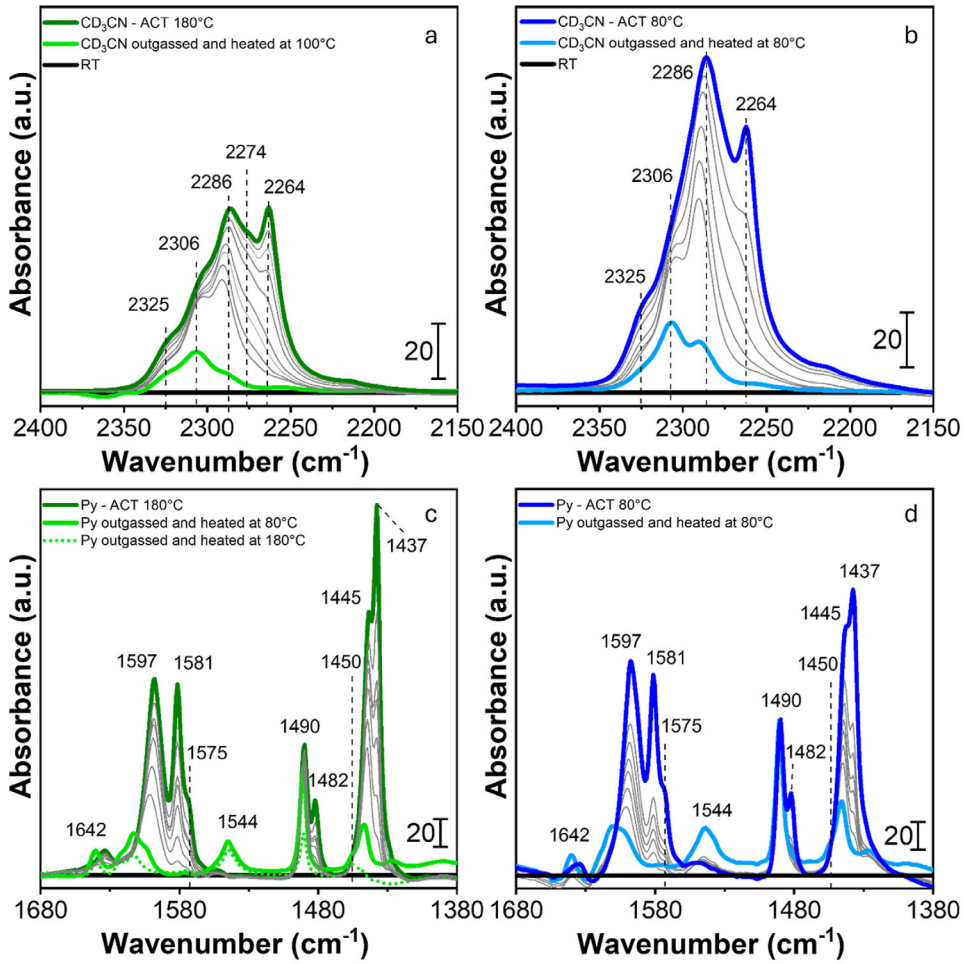

Figure 4. IR spectra of FULCAT®-22 F after adsorption of 15 mbar CD_3CN (a and b) and 26 mbar pyridine (c and d) on the previously evacuated sample at 180 °C (a and c) and 80 °C (b and d). Dark coloured, grey, light coloured and black lines represent the maximum adsorption, the progressive outgassing, the reactivated and the fully evacuated samples, respectively. The spectra were normalised by means of the optical density (OD) and plotted by subtracting the spectrum of the evacuated material (see Supporting Information).

ple activated at 400 °C, which is an ideal working condition for IR spectroscopy, was also studied in the same way for comparison.

The interaction of CO with the sample activated at the three temperatures was first studied by dosing a proper amount of gas (~60 mbar) into the cell and cooling down to −196 °C with liquid nitrogen (see Supporting Information, e.g., Figure S20, for additional information). In all three cases, two main bands at 2158 and 2140 cm^{-1} were observed, attributed to the interaction with weakly acidic silanols and liquid-like CO, respectively. Some additional bands at higher wavenumbers start to appear at low CO pressures, but the broadness and the low intensity of the signals make it difficult to make a correct assignment (for details, see Figure S20 and section S7). To better identify the presence of BAS and LAS in the material, other stronger basic molecular probes as CD_3CN and pyridine, were employed (Figure 4).

The interaction of CD_3CN with the sample activated at 180 °C and 80 °C is shown in Figure 4A,B. The adsorption of CD_3CN at RT on the samples resulted in the appearance of numerous bands shifted to higher frequencies with respect to the original C—N stretching mode of free CD_3CN (2263 cm^{-1}), indicating the presence of several sites having different acidity.

In both samples, two sharp bands can be observed at 2286 and 2264 cm^{-1}. The intensity of these signals varies according to the activation: in the sample activated at 180 °C, the two bands reach similar intensities, whereas in the sample activated at 80 °C, the one at 2286 cm^{-1} is more intense. Additionally, for the 180 °C activated sample, the 2286 cm^{-1} band is broader, suggesting the presence of an additional signal at lower wavenumbers (~2274 cm^{-1}) which is easily desorbed during outgassing. As the pressure decreases, the 2264 cm^{-1} band quickly disappears, while the 2286 cm^{-1} signal is more resistant and shifts slightly to 2290 cm^{-1}. The higher strength of this latter band is also highlighted by its persistence when the sample is reheated (see the light-coloured lines in Figure 4A,B). The behavior and position of the band suggest that the 2264 cm^{-1} is due to liquid-like CD_3CN, while the 2286 cm^{-1} one is tentatively assigned to the interaction of the molecular probe with the BAS of the material, which can be both structural and/or originate from the water polarization. Differently, the shoulder visible in the 180 °C activated spectra at 2274 cm^{-1} is due to the interaction with silanols. Therefore, in

the OH stretching region (Figure S21c,e), the 3748 cm^{-1} band is consumed and shifted to a broader signal at 3425 cm^{-1}.

At wavenumbers higher than 2286 cm^{-1}, both the samples display the presence of one main signal at 2306 cm^{-1} together with the presence of a shoulder having the apparent maximum at around 2325 cm^{-1}. However, also in this case the broadness of the bands suggests the presence of several sites. Both signals result to be stable upon outgassing and only by re-heating the sample, the intensities visibly decrease. Taking into consideration the large shift to higher frequencies of those bands (respectively, $\Delta\nu = +43$ and $\Delta\nu = +62$ cm^{-1} with respect to 2263 cm^{-1}) and the high stability to evacuation, those signals could be assigned to the interaction of CD_3CN with LAS. The broadness of the bands suggests the existence of different LASs on the samples, whose precise assignment is not straightforward (a tentative assignment is reporting in the Supporting Information, Section S7-Adsorption of CD_3CN).

Comparing the samples activated at 80 °C and 180 °C, a slight difference in BAS and LAS present in the sample can be observed. As a matter of fact, in the less activated sample the relative intensity of BAS seems to prevail with respect to both silanols and Lewis ones. Upon increasing the activation temperature, the prevalence of BAS slowly decreases as underlined by the appearance of 2274 cm^{-1} silanols band and by the lower intensity of the 2286 cm^{-1} signal. This tendency is confirmed by repeating the experiment on the sample activated at 400 °C (Figure S21a,b). In this case, there is a prevalence of silanols and liquid-like bands at 2274 and 2264 cm^{-1}, respectively, while the band relative to BAS further decreases and slightly shifts to 2290 cm^{-1}. A possible explanation of this behavior is due to the different water contents of the sample activated at the three temperatures. As previously explained, it is well known that part of the BASs in montmorillonite comes from the polarization of the H_2O molecule and therefore prevails at low activation temperature.[18] When the activation temperature reaches 400 °C, the residual BAS signal at 2290 cm^{-1} is likely to be due to some structural BAS sites rather than to the one coming from the polarization of H_2O, which are expected to be almost completely outgassed.

The acid sites present in FULCAT®-22 F were further studied by dosing pyridine (Py) on the sample activated at 180 °C and 80 °C Figure 4C,D. The interaction of pyridine with the samples led to the appearance of numerous signals in the 1680–1380 cm^{-1} spectral range, where the 8a, 8b, 19a, and 19b ring-stretching modes of Py can be appreciated.[39,60]

In both spectra, the bands at 1581, 1482, and 1437 cm^{-1}, which are easily desorbed during the outgassing, can be reasonably assigned to modes 8a, 19a, and 19b of physiosorbed Py.[39,61,62] Additionally, the hydrogen-bonded Py to weakly acidic silanols is observed at 1597 (8a) and 1445 cm^{-1} (19a) (see Table S3 for the assignments).[18,39,61] As expected, those bands result in being more stable during the outgassing with respect to the physiosorbed ones. In the OH stretching region (Figure S22c,e), the interaction with silanols caused the erosion of 3748 cm^{-1} bands and the formation of a strong and broad absorption centered at about 3000 cm^{-1} ($\Delta\nu \sim 700$ cm^{-1}).[62] In the high frequency region, the appearance in the 3200–3000 cm^{-1} spectral range of different CH stretching bands is also observed. In both spectra, two weak signals at 1575 and 1450 cm^{-1} present as shoulders of the more intense bands at 1581 and 1445 cm^{-1} can be distinguished. Those bands can be attributed to the interaction with LAS (L-Py) (8b and 19b modes, respectively).[39,61] In addition, the 1490 cm^{-1} signal can be due to the 19a mode of L-Py, although it is also attributed to the interaction with both LAS and BAS.[18,39,63] Interestingly, by reactivating the samples, the silanols bands at 1597 and 1445 cm^{-1} decrease drastically, while the 1490 cm^{-1} band seems to remain almost unchanged. However, the most interesting phenomenon is the appearance of a band at 1544 cm^{-1}, which was completely absent in the adsorption spectra performed on the sample activated at 180 °C and not very intense in the one activated at 80 °C. The appearance of this band is characteristic of the formation of the pyridinium ion generated by the interaction with BAS.[18,63] Also, one additional band at 1642 cm^{-1}, due to the 8a or 8b mode of BAS, appeared.[60] The appearance of BAS only during the outgassing or the reactivation of the sample seems to be a rather unusual phenomenon. A possible explanation could be that the pyridine molecules firstly interact with residual physiosorbed or interlayer water molecules present in the clay through the formation of a bond between the nitrogen atom of pyridine and one of the hydrogen atoms of water.[64] During the outgassing, those water molecules start to be evacuated, facilitating the interaction with the structural BAS of the samples. However, this pyridine "washing" alters the amount of H_2O present in the sample, which is responsible for the formation of the H^+ BAS through the polarization of interlayer cations, making it impossible to study the true nature of the sample. For this reason, pyridine is probably not the most suitable molecular probe to detect differences in BAS present in the samples activated at different temperatures.

By looking at the spectra of the sample activated at 400 °C (Figure S22a,b) the same bands except for the one related to BAS appear upon interaction with pyridine. The absence of those signals is probably due to the low water content, and consequently low BAS present in the sample which can be further reduced by the "pyridine washing". The low concentration of BAS sites, the partial loss of structure due to thermal treatment and the hindrance of the pyridine molecule probably prevent the appearance of any bands relative to BAS, which was otherwise observed for CD_3CN on the 400 °C activated sample (Figure S21b). Only the interaction with a strong and smaller molecule as NH_3 (kinetic diameter 5.7 Å and 2.6 Å for pyridine and NH_3, respectively)[65,66] reveals the presence of some residual more easily accessible structural BAS (see Supporting Information, e.g., Figure S23, for additional information).

Lastly, in order to study the accessibility of the different acid sites to 1-hexanol and to simulate a situation closer to the catalytic conditions, heptanenitrile ($C_7H_{13}N$) was dosed to the sample activated at 180 °C (Figures S24 and S25). Upon interaction with $C_7H_{13}N$, one main band at 2273 cm^{-1}, together with two shoulders at around 2290 and 2310 cm^{-1}, appears. By comparing those signals with the one obtained from CD_3CN adsorption (see Supporting Information for further details), the former one was assigned to BAS, while the latter one to LAS. The presence of the same band trend observed for CD_3CN, having very

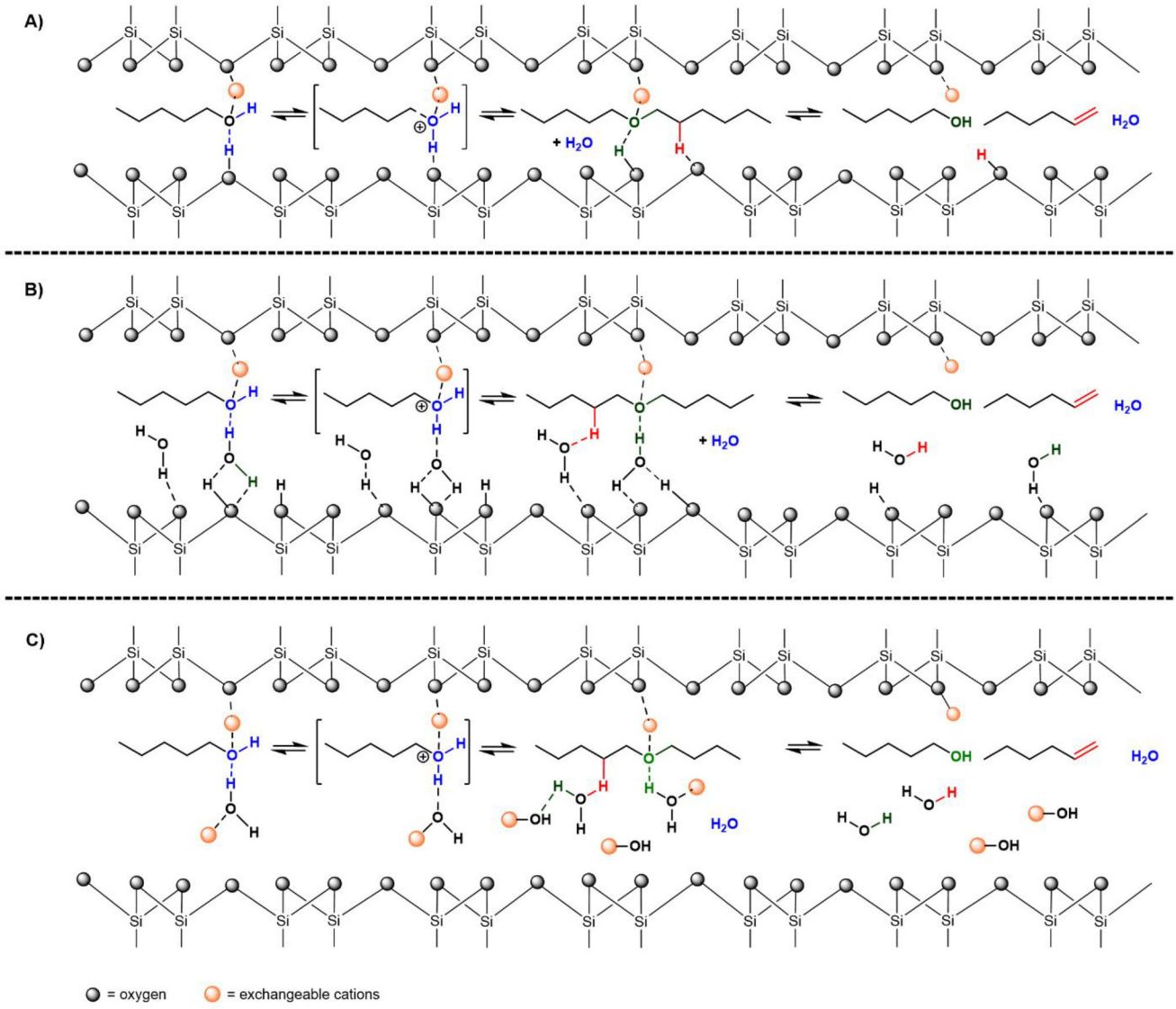

Figure 5. Postulated mechanism for the dehydration of primary alcohols by acid-pretreated montmorillonites, based on experimental tests and analytical work. 1-Hexanol was chosen as the model substrate, and for simplification, only the interlayer region with the Si^{4+} tetrahedral layout is shown. (A) Dehydration facilitated by protonated bridging oxygens, (B) dehydration involving protonated bridging oxygens and water molecules as proton donors, and (C) dehydration mediated by water molecules as proton donors.

similar relative intensities, highlighted that the different acid sites are all available to hexanol, used for the catalytic test, and the hindrance of the molecule is not playing a role in their accessibility.

3.4. Postulated Reaction Mechanisms for the Dehydration of Primary Alcohols

Based on the analytical and experimental results, we propose potential mechanisms for the dehydration of primary alcohols catalyzed by acid-pretreated montmorillonites. It should be added that these mechanisms described in the following represent only a few plausible pathways based on conceivable interactions of specific moieties in the montmorillonite catalyst with the substrate (shown in Figure 5) and have not been confirmed by spectroscopic methods yet. Our recent work indicates that under mild conditions, ether formation occurs first, followed by elimination to yield the corresponding alkene. We assume that a similar pathway is present in this case when using such a montmorillonite-type catalyst. Ether formation may proceed via various mechanisms; here, we will only discuss three potential catalytic pathways. Accordingly, ether formation can (A) be facilitated by protonated bridging oxygens, (B) involve both protonated bridging oxygens and water molecules as proton donors, and (C) be mediated solely by water molecules acting as proton donors (Figure 5). The subsequent elimination step yields one equivalent of alcohol and 1-alkene. Under the applied reaction conditions (leading to a thermodynamically controlled process), the initially formed 1-alkene undergoes rapid isomerization, resulting in a mixture of alkene isomers. As described in Figure 5B,C, water from the interlayer can play

an active role in the elimination reaction. It can be activated either by Brønsted acid sites (Figure 5B) or by Lewis acid sites (Figure 5C). Since the reaction is reversible, hydration of the alkene products, as suggested in the case of tertiary alcohols, cannot be excluded. However, as the alkene products are continuously removed from the reaction mixture, the equilibrium is shifted toward the formation of alkenes.

4. Conclusions

A commercial acid-leached bentonite (FULCAT®-22 F) turned out to facilitate efficiently the dehydration reaction of a range of substituted alcohols under energy-saving conditions at much lower temperatures than most "traditional catalysts" for this purpose. Dehydration of 2-methyl-2-hexanol was observed to occur at 60 °C, while the dehydration of a primary alcohol such as 1-hexanol was noted to take place at 150–180 °C. This temperature is relatively mild in comparison to the typical dehydration of primary alcohols, which often occurs at temperatures exceeding 300 °C. While at 2 mol%, an alkene formation of 8% was observed with the best Brønsted acid (TfOH), a yield of 52% was observed with the studied material FULCAT®-22 F, representing a 6.5-fold increase. Furthermore, dehydration of primary alcohols with different chain lengths also proceeds successfully. A stability and recycling study was conducted, demonstrating 10 catalytic cycles without any loss of activity. After each reaction, the reaction vessel was filled, necessitating, however, recycling of the catalyst after cycle 6. While the yields remained fairly constant during cycles 1–6, a lower yield was then observed in cycle 7 after the recycling of the catalyst. In subsequent cycles, then the yields returned to the range of the average value.

In order to rationalize this unexpected high catalytic activity being superior to "classic" Brønsted acids with much lower pKa values, the catalyst was deeply characterized using both fundamental and advanced characterization methods. In this regard, VT-XRD evidenced the prevalence of montmorillonite structure and impurities of quartz, together with a probable decrease in the basal parameters by increasing temperature due to the evacuation of the water present in the structure. TGA analysis shows that water removal in the structure occurs between RT and 200 °C, in perfect agreement with VT-XRD results. BET and PSD analysis evidenced a decrease in the surface area and a slight modification in the micropores present in the material by increasing the temperature. Due to EDX, Fe, Mg, and K results to be the most abundant elements present in the structure after the acid treatment performed to prepare this commercial sample. The deep spectroscopic analysis, carried out with different molecular probes of variable basicity (CO, CD_3CN, Py, and NH_3), revealed a modification of the BAS and LAS present in the samples activated at different temperatures. In particular, CD_3CN dosage revealed, on one side, the presence of different LAS in the sample, on the other the prevalence of BAS when the sample is activated at the lowest temperature (80 °C). These BAS are probably mainly H^+ sites coming from water polarised by the cations in the interlayer, which explains why these species decrease with increasing activation temperature (180 °C and 400 °C). However, when the sample is fully activated (400 °C) along with LAS, some residual BAS were also observed, indicating that some residual structural BAS are likely to be present in the sample. On the other hand, pyridine results to be not the most suitable molecular probe to detect different acidities of the samples activated at different temperatures due to its interaction with H_2O present in the clay and the consequent alteration of the BAS sites. Lastly, the use of heptanenitrile showed that the different acid sites are all available to hexanol, the reactant in catalytic testing, and molecule hindrance plays no role in their accessibility.

Author Contributions

The manuscript was written with contributions of all authors.

Acknowledgments

The authors acknowledge Dr. Gianluca Fiore for the help in carrying out VT-XRD measurements and Dr. Francesca Rosso for her help in the representation of the structure of the bentonite. MC, MD, VC, and FB acknowledge support from the Project CH4.0 under the MUR program "Dipartimenti di Eccellenza 2023–2027" (CUP: D13C22003520001) and the NODES project funded by the European Union – NextGenerationEU, Mission 4 Component 1.5 – ECS00000036 – CUP D17G22000150001. The authors also acknowledge financial support from the European Union's Horizon 2020 research and innovation programme under Grant Agreement No. 101022633. This work is supported by Japan Science and Technology Agency (JST) under Grant Agreement No. JPMJSC2102. This project is developed in the frame of a Mission Innovation Challenge.

Open access publishing facilitated by Universita degli Studi di Torino, as part of the Wiley - CRUI-CARE agreement.

Conflict of Interests

The authors declare no conflict of interest.

Data Availability Statement

The data that support the findings of this study are available from the corresponding author upon reasonable request.

Keywords: Alcohols · Alkenes · Clay · Dehydration · Montmorillonite

[1] T. Marzi, V. Knappertsbusch, A. Grevé, G. Deerberg, C. Doetsch, E. Weidner, *Chemie Ing. Tech.* **2018**, *90*, 1374–1383.
[2] K. Weissermel, H. Arpe, *Industrial Organic Chemistry*, Wiley-VCH, Weinheim **2010**.
[3] E. W. Kuipers, I. H. Vinkenburg, H. Oosterbeek, *J. Catal.* **1995**, *152*, 137–146.
[4] B. Kamm, *Angew. Chem., Int. Ed.* **2007**, *46*, 5056–5058.
[5] Q. Zhang, J. Kang, Y. Wang, *ChemCatChem* **2010**, *2*, 1030–1058.
[6] E. de Smit, B. M. Weckhuysen, *Chem. Soc. Rev.* **2008**, *37*, 2758.

[7] Y. Chen, J. Wei, M. S. Duyar, V. V. Ordomsky, A. Y. Khodakov, J. Liu, *Chem. Soc. Rev.* **2021**, *50*, 2337–2366.
[8] T. Haas, R. Krause, R. Weber, M. Demler, G. Schmid, *Nat. Catal.* **2018**, *1*, 32–39.
[9] W. Brandenberg, A. Galat, *J. Am. Chem. Soc.* **1950**, *72*, 3275–3276.
[10] J. T. Vossen, A. J. Vorholt, W. Leitner, *ACS Sustainable Chem. Eng.* **2022**, *10*, 5922–5931.
[11] A. Allahverdiyev, J. Yang, H. Gröger, *Green Chem.* **2024**, *26*, 7869–7878.
[12] N. Makgoba, T. Sakuneka, J. Koortzen, C. Vanschalkwyk, J. Botha, C. Nicolaides, *Appl. Catal. A Gen.* **2006**, *297*, 145–150.
[13] I. Takahara, M. Saito, M. Inaba, K. Murata, *Catal. Letters* **2005**, *105*, 249–252.
[14] K. Stanciakova, B. M. Weckhuysen, *Trends Chem* **2021**, *3*, 456–468.
[15] J. H. Lee, S. B. Hong, *Appl. Catal. B Environ.* **2021**, *280*, 119446.
[16] S. Moon, H.-J. Chae, M. B. Park, *Appl. Catal. A Gen.* **2018**, *553*, 15–23.
[17] J. Cuevas, M. Á. Cabrera, C. Fernández, C. Mota-Heredia, R. Fernández, E. Torres, M. J. Turrero, A. I. Ruiz, *Minerals* **2022**, *12*, 772.
[18] D. Haffad, A. Chambellan, J. C. Lavalley, *Catal. Lett.* **1998**, *54*, 227–233.
[19] D. R. Brown, C. N. Rhodes, *Catal. Lett.* **1997**, *45*, 35–40.
[20] D. Borah, H. Nath, H. Saikia, *Rev. Inorg. Chem.* **2022**, *42*, 265–282.
[21] X. Zhang, J. Wang, L. Wang, Z. Li, W. Hu, Y. Dai, Y. Kou, S. Lei, Q. Li, W. Zhang, H. Li, R. Wang, Q. Feng, *Fuel* **2023**, *333*, 126621.
[22] M. Sklenár, V. Danielik, P. Hudec, *Chem. Pap.* **2017**, *71*, 1453–1461.
[23] G. Kostrab, M. Lovič, A. Turan, P. Hudec, A. Kaszonyi, M. Bajus, J. Uhlár, P. Lehocký, D. Mravec, *Catal. Commun.* **2012**, *18*, 176–181.
[24] N. J. Venkatesha, Y. S. Bhat, B. S. Jai Prakash, *RSC Adv.* **2015**, *5*, 69348–69355.
[25] K. Shimizu, T. Higuchi, E. Takasugi, T. Hatamachi, T. Kodama, A. Satsuma, *J. Mol. Catal. A Chem.* **2008**, *284*, 89–96.
[26] J. M. Gnaim, R. A. Sheldon, *Tetrahedron Lett.* **2004**, *45*, 9397–9399.
[27] M. K. Yadav, C. D. Chudasama, R. V. Jasra, *J. Mol. Catal. A Chem.* **2004**, *216*, 51–59.
[28] M. Bolognini, F. Cavani, M. Cimini, L. D. Pozzo, L. Maselli, D. Venerito, F. Pizzoli, G. Veronesi, *Comptes. Rendus. Chim.* **2004**, *7*, 143–150.
[29] M. Raimondo, A. De Stefanis, G. Perez, A. A. Tomlinson, *Appl. Catal. A Gen.* **1998**, *171*, 85–97.
[30] V. R. Madduluri, N. K. Katari, N. Peddinti, V. K. Velpula, D. R. Burri, S. R. R. Kamaraju, S. B. Jonnalagadda, *Res. Chem. Intermed.* **2018**, *44*, 7619–7639.
[31] J. A. Ballantine, J. H. Purnell, J. M. Thomas, *Clay Miner.* **1983**, *18*, 347–356.
[32] J. M. Adams, *Appl. Clay Sci.* **1987**, *2*, 309–342.
[33] P. Kumar, R. V. Jasra, T. S. G. Bhat, *Ind. Eng. Chem. Res.* **1995**, *34*, 1440–1448.
[34] J. Temuujin, T. Jadambaa, G. Burmaa, S. Erdenechimeg, J. Amarsanaa, K. J. D. MacKenzie, *Ceram. Int.* **2004**, *30*, 251–255.
[35] M. Gupta, J. J. Spivey, in *New Futur. Dev. Catal.* (Ed: S. L. Suib), Elsevier, Amsterdam **2013**, pp. 87–126.
[36] D. M. Reinoso, S. Angeletti, P. M. Cervellini, D. E. Boldrini, *Brazilian J. Chem. Eng.* **2020**, *37*, 679–690.
[37] J. Rouquerol, P. Llewellyn, F. Rouquerol, *Stud. Surf. Sci. Catal.* **2007**, *106*, 49–56.
[38] A. Zecchina, S. Bordiga, G. Spoto, L. Marchese, G. Petrini, G. Leofanti, M. Padovan, *J. Phys. Chem.* **1992**, *96*, 4985–4990.
[39] F. Bonino, A. Damin, S. Bordiga, C. Lamberti, A. Zecchina, *Langmuir* **2003**, *19*, 2155–2161.
[40] S. Bordiga, I. Roggero, P. Ugliengo, A. Zecchina, V. Bolis, G. Artioli, R. Buzzoni, G. Marra, F. Rivetti, G. Spanò, C. Lamberti, *J. Chem. Soc. Dalt. Trans.* **2000**, 3921–3929.
[41] T. L. Lohr, Z. Li, T. J. Marks, *Acc. Chem. Res.* **2016**, *49*, 824–834.
[42] C. K. Narula, Z. Li, E. M. Casbeer, R. A. Geiger, M. Moses-Debusk, M. Keller, M. V. Buchanan, B. H. Davison, *Sci. Rep.* **2015**, *5*, 16039.
[43] E. Medina, R. Bringué, J. Tejero, M. Iborra, C. Fité, *Appl. Catal. A Gen.* **2010**, *374*, 41–47.
[44] C. Casas, R. Bringué, E. Ramírez, M. Iborra, J. Tejero, *Appl. Catal. A Gen.* **2011**, *396*, 129–139.
[45] R. J. J. Nel, A. de Klerk, *Ind. Eng. Chem. Res.* **2009**, *48*, 5230–5238.
[46] D. H. Hong, M. N. Gebresillase, J. G. Seo, *J. Clean. Prod.* **2024**, *451*, 141994.
[47] A. Lee, G. Xiao, P. Xiao, K. Joshi, R. Singh, P. A. Webley, *Energy Procedia.* **2011**, *4*, 1199–1206.
[48] J. Bi, X. Guo, M. Liu, X. Wang, *Catal. Today* **2010**, *149*, 143–147.
[49] A. W. Lepore, Z. Li, B. H. Davison, G.-S. Foo, Z. Wu, C. K. Narula, *Ind. Eng. Chem. Res.* **2017**, *56*, 4302–4308.
[50] A. de Reviere, D. Gunst, M. K. Sabbe, M.-F. Reyniers, A. Verberckmoes, *Catal. Sci. Technol.* **2021**, *11*, 2540–2559.
[51] M. Ngcobo, P. R. Makgwane, M. K. Mathe, *Appl. Catal. O Open* **2024**, *193*, 206976.
[52] P. Iadrat, K. Yomthong, C. Rodaum, P. Pornsetmetakul, A. Thivasasith, A. Prasertsab, X. Fan, T. Sooknoi, C. Wattanakit, *Fuel* **2023**, *338*, 127208.
[53] D.-W. Lee, M.-H. Jin, J.-H. Park, Y.-J. Lee, Y.-C. Choi, Y.-E. Kim, K. Y. Koo, J. C. Park, M. H. Youn, D. H. Chun, *Fuel* **2023**, *333*, 126367.
[54] I. S. Fatimah, N. Narsito, K. Wijaya, *ITB J. Sci.* **2011**, *43A*, 123–138.
[55] Z. Orolínová, A. Mockovčiaková, S. Dolinská, J. Briančin, *Arch. Tech. Sci.* **2012**, *2*, 97–104.
[56] T.-J. Park, D. Seoung, *Nucl. Eng. Technol.* **2021**, *53*, 1511–1518.
[57] M. Thommes, K. Kaneko, A. V. Neimark, J. P. Olivier, F. Rodriguez-Reinoso, J. Rouquerol, K. S. W. Sing, *Pure Appl. Chem.* **2015**, *87*, 1051–1069.
[58] R. Přikryl, Z. Weishauptová, *Appl. Clay Sci.* **2010**, *47*, 163–170.
[59] S. Bordiga, C. Lamberti, F. Bonino, A. Travert, F. Thibault-Starzyk, *Chem. Soc. Rev.* **2015**, *44*, 7262–7341.
[60] C. Morterra, G. Magnacca, *Catal. Today* **1996**, *27*, 497–532.
[61] S. Bodoardo, F. Figueras, E. Garrone, *J. Catal.* **1994**, *147*, 223–230.
[62] R. Buzzoni, S. Bordiga, G. Ricchiardi, C. Lamberti, A. Zecchina, G. Bellussi, *Langmuir* **1996**, *12*, 930–940.
[63] D. Tichit, F. Fajula, F. Figueras, J. Bousquet, C. Gueguen, in *Catal. by Acids Bases* (Eds: B. Imelik, C. Naccache, G. Coudurier, Y. B. Taarit, J. C. Vedrine), *Stud. Surf. Sci. Catal*, Elsevier, Amsterdam **1985**, pp. 351–360.
[64] K. K. Zborowski, J. Poater, *ACS Omega* **2021**, *6*, 24693–24699.
[65] D. W. Breck, *Zeolite Mol. Sieves: Struct., Chem. Use*, Wiley, New York **1973**, 771.
[66] P. Bräuer, P. L. Ng, O. Situmorang, I. Hitchcock, C. D'agostino, *RSC Adv.* **2017**, *7*, 52604–52613.

Manuscript received: February 25, 2025
Revised manuscript received: June 11, 2025
Accepted manuscript online: June 13, 2025
Version of record online: ■■, ■■